Cell Reports

Article

ARF19 acts as a transient auxin response enhancer during root gravitropism

Graphical abstract

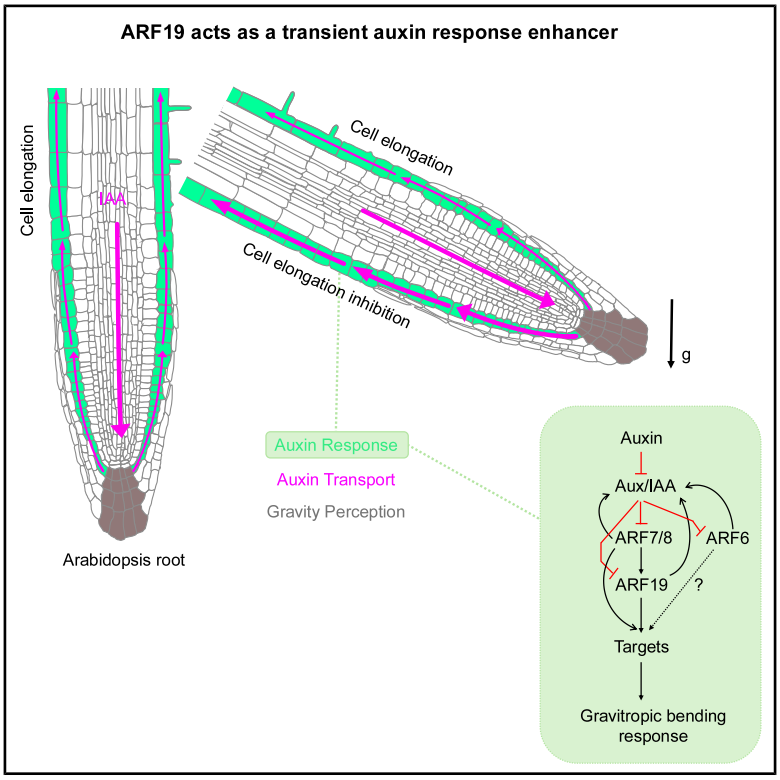

Authors

Erfan Ghafouri, Kristine Hill, Nathan Mellor, ..., Malcolm J. Bennett, Tatsuaki Goh, Rahul A. Bhosale

Correspondence

malcolm.bennett@nottingham.ac.uk (M.J.B.), goh@bs.naist.jp (T.G.), rahul.bhosale@nottingham.ac.uk (R.A.B.)

In brief

Root gravitropism depends on precise auxin signaling mediated by auxin response factors (ARFs). This study reveals that ARF7 and ARF8 drive rapid, transient activation of ARF19 during gravitropic responses, with ARF19 acting as an auxin response enhancer for a subset of shared ARF7 target genes.

Highlights

- *ARF19* is rapidly and transiently induced during gravitropism
- ARF7 and ARF8 can bind the ARF19 promoter to regulate its auxin-inducible expression
- ARF7 and ARF19 co-regulate gravitropism together with ARF6 and ARF8
- ARF7 can substitute for ARF19 but not vice versa

Ghafouri et al., 2026, Cell Reports *45*, 117555
June 23, 2026
https://doi.org/10.1016/j.celrep.2026.117555

CellPress

Cell Reports

CellPress
OPEN ACCESS

Article

ARF19 acts as a transient auxin response enhancer during root gravitropism

Erfan Ghafouri,[1,10] Kristine Hill,[1,2,10] Nathan Mellor,[1,2] Nicola Leftley,[1,2] Ethel Mendocilla Sato,[1,2,3] Jason Banda,[1] Aneesh Lale,[1] Atish Bansod,[1] Michael Wilson,[1,2] Bipin Kumar Pandey,[1] Jekaterina Truskina,[1,7] Jaesung Oh,[1,11] Jingyi Han,[1] Azad Kilic,[1,12] Darren Wells,[1,2] Benjamin Péret,[1,2,13] Ranjan Swarup,[1,2] Gretchen Hagen,[4] Tom Guilfoyle,[4] Kris Vissenberg,[3,5] Thomas Berleth,[6] Teva Vernoux,[7] Anthony Bishopp,[1,2] Hidehiro Fukaki,[8] Malcolm J. Bennett,[1,2,*] Tatsuaki Goh,[1,2,9,*] and Rahul A. Bhosale[1,2,14,*]

[1]Plant and Crop Sciences, School of Biosciences, University of Nottingham, Nottingham LE12 5RD, UK
[2]Centre for Plant Integrative Biology (CPIB), University of Nottingham, Nottingham LE12 5RD, UK
[3]Biology Department, Integrated Molecular Plant Physiology Research, University of Antwerp, Groenenborgerlaan 171, 2020 Antwerpen, Belgium
[4]Department of Biochemistry, University of Missouri-Columbia, Columbia, MO 65211, USA
[5]Plant Biochemistry & Biotechnology Lab, Department of Agriculture, Hellenic Mediterranean University, Stavromenos PC 71410 Heraklion, Crete, Greece
[6]Department of Cell and Systems Biology, University of Toronto, 25 Willcocks Street, Toronto, ON M5S 3B2, Canada
[7]Laboratoire Reproduction et Développement des Plantes, University Lyon, ENS de Lyon, CNRS, INRAE, Inria, Lyon, France
[8]Department of Biology, Graduate School of Science, Kobe University, 1-1 Rokkodai, Kobe 657-8501, Japan
[9]Graduate School of Science and Technology, Nara Institute of Science and Technology, 8916-5 Takayama, Ikoma 630-0192, Japan
[10]These authors contributed equally
[11]Present address: Institute of Plasma Technology, Korea Institute of Fusion Energy, 37 Dongjangsan-Ro, Gunsan-Si, Jeonbuk-Do, Republic of Korea
[12]Present address: Artuklu Directorate of District Agriculture and Forestry, Ministry of Agriculture and Forestry, 47100 Mardin, Türkiye
[13]Present address: IPSiM, University of Montpellier, CNRS, INRAE, Institut Agro, Montpellier, France
[14]Lead contact
*Correspondence: malcolm.bennett@nottingham.ac.uk (M.J.B.), goh@bs.naist.jp (T.G.), rahul.bhosale@nottingham.ac.uk (R.A.B.)
https://doi.org/10.1016/j.celrep.2026.117555

SUMMARY

Root gravitropism is regulated by an auxin gradient, causing the root to reorient downwards with gravity. Transcriptional activator auxin response factors (ARFs), such as ARF5, ARF6, ARF7, ARF8, and ARF19, play key roles in auxin signaling in seedling root tissues. ARF7 and ARF19 are both required for root gravitropism, but their regulatory relationship with each other and other activating ARFs remains unknown. Here, we identify that rapid and transient upregulation of ARF19 during gravitropic stimulus is functionally important. ARF7 and ARF8 are required to activate *ARF19* upregulation via auxin response elements (AuxREs) in its promoter, while our data indicate that ARF19 does not self-activate. ARF7 can replace ARF19 but not vice versa. Although ARF7 shares overlapping targets with ARF19, they also have distinct functionally important targets, such as ARF19. Our results show that ARF7 and ARF19 have sub-functionalized, with ARF19 acting as an auxin response enhancer for a subset of ARF7 target genes.

INTRODUCTION

Land plants employ gravitropism to orient their growth and development relative to gravity. For example, newly germinating seedlings employ root gravitropism to establish themselves in soil and forage for water and nutrients. The root gravitropic response involves three sequential steps: gravity perception, signal transduction, and differential root growth. Changes in root orientation relative to gravity is sensed in columella cells at the root tip, triggering the formation of a lateral auxin gradient, which the root cap transports to epidermal cells in the elongation zone.[1–3] This differential accumulation of auxin in these epidermal cells on the lower side of roots causes cell expansion to be reduced relative to the upper side, resulting in the root growth re-orienting downwards.[4,5]

Auxin-responsive gene expression in plants is co-regulated by auxin/indole-3-acetic acid (Aux/IAA) and auxin response factor (ARF) family proteins. Auxin promotes the interaction between its co-receptors transport inhibitor response 1 (TIR1)/auxin-signaling F-box (AFB) and Aux/IAA repressor proteins,[6–8] resulting in their ubiquitination and degradation of Aux/IAAs.[9] Aux/IAA degradation de-represses interacting ARFs, thereby activating transcription of downstream genes.[10,11] Several activating ARF genes themselves are auxin-responsive.[12,13] This regulatory arrangement creates the potential for feedforward loops.

Previous research in *Arabidopsis* sp. revealed that among the 23 members of ARFs, ARF7 and ARF19 are both required for root gravitropism, where ARF19 (but not ARF7) is auxin-inducible.[13] The topology of their regulatory relationship is likely to profoundly impact the dynamics and magnitude of ARF7-ARF19-mediated auxin-responsive gene expression. However, the regulatory relationship of ARF7 and ARF19 and their auxin-responsive gene targets remains unclear. Additionally, other transcriptional activator ARFs (such as ARF5, ARF6, and ARF8) are known to be essential for regulating auxin signaling in seedling tissues.[14] Whether these ARFs have any regulatory relationship with ARF7 and ARF19 in controlling root gravitropism is currently not known.

Here, we report that during root gravitropism, auxin-responsive genes are transiently induced prior to the sequential induction of genes involved in cytokinin signaling and cell-wall-related processes. Transcript profiling revealed that among activating ARFs, only *ARF19* expression is induced and only transiently. Mathematical modeling backed by experimental validation confirms that ARF7 controls *ARF19* expression, but ARF19 cannot activate itself. Functional studies demonstrate the importance of auxin-mediated upregulation of *ARF19* during a root gravitropic response. Transcript analysis reveals that ARF19 regulates the expression of only a subset of ARF7 targets, indicating that the former protein has sub-functionalized. We conclude by discussing the implications of this regulatory network arrangement on auxin response dynamics.

RESULTS

Root gravitropism triggers sequential induction of hormone and then cell wall genes

ARF7 and ARF19 are both required for root gravitropism,[13] since *arf7-1arf19-1* double mutant roots exhibit a reduced gravity response, while *arf7-1* and *arf19-1* single mutants do not (Figures 1A and 1B). To understand ARF7-ARF19-mediated auxin-responsive gene expression during root gravitropism, *Arabidopsis thaliana* wild type (Col-0 ecotype) and *arf7-1arf19-1* mutant root tips were collected at 0, 15, 30, 60, 120, 240, and 480 min after gravistimulation and subjected to transcriptome analysis (see STAR Methods). In total, 637 genes were found to be differentially expressed (p-value <0.05, Benjamini-Hochberg FDR correction and $-1.5 \leq$ fold change ≥ 1.5) across both time series, when each time point was compared against the 0 min time point for Col-0 time series and respective time points were compared between Col-0 and *arf7arf19-1* mutant (Table S1). Gene Ontology (GO) enrichment (Table S2) and prefiltering of semantically redundant GO terms showed that auxin response genes were rapidly induced 15 min after gravistimulation, followed by the cytokinin-signaling pathway and cytokinin response genes at 60 min (Figure 1C). Subsequently, cell wall organization or biogenesis, cell-cell junction assembly and cell wall organization related genes were induced at 120, 240, and 480 min, respectively (Figure 1C).

The root gravitropic response is known to be controlled in specific tissues and developmental zones. We investigated how gravistimulus-induced temporal gene expression changes relate to these root tissues and developmental stages. In this context, we assessed peak expression of differentially expressed genes per time point using root cell type (marker) and developmental stage (zone) specific gene expression data[15] (Figure S1). This analysis revealed that genes are predominantly expressed in the lateral root cap and epidermal cells in the meristematic region (slices 1–6) within 15 min, then in the epidermal cells in the late meristem and elongating cells region (slice 5, 7–10) at 30 and 60 min time points, and later in the cortex in the elongation zone at later time points of 120 and 240 min. These spatial transcriptomic changes are consistent with the sequential events (i.e., auxin gradient formation, signal transduction, and root bending) observed during root gravitropism. Hence, auxin transcriptionally regulates a cascade of spatial and temporal events during a root gravitropic response.

Auxin-inducible *ARF19* expression is required for root gravitropism

A transient lateral auxin gradient is known to control root gravitropism.[3] Consistently, our time series transcriptome analysis identified known auxin signaling and response genes rapidly and transiently induced following a gravity stimulus (Table S1; Figures S1 and S2). We specifically studied the transcript levels of activating ARFs *ARF5*, *ARF6*, *ARF7*, *ARF8*, and *ARF19* that regulate the majority of auxin-responsive genes in seedling root tissues.[16] Interestingly, only *ARF19* transcript levels were rapidly upregulated between 15 and 30 min after gravistimulation and remained elevated for up to 60 min before starting to decrease (Figure 2A), suggesting that *ARF19* is rapidly and transiently induced by the lateral auxin gradient during a gravitropic response.

To investigate auxin response and spatiotemporal regulation of ARFs, transcriptional reporters for different activating ARFs were compared with p*DR5*::Venus expression following 3 h of gravistimulation. This analysis confirmed that only p*ARF19*::Venus expression was differentially upregulated on the lower vs. upper side of roots during a gravitropic bending response, correlating with lateral auxin gradient formation (Figures S3, 2B, and 2C). We next assessed the temporal dynamics of p*DR5*::Venus and p*ARF19*::Venus expression at 0, 1, 2, and 3 h after gravistimulation. Asymmetric expression of both *DR5* and *ARF19* were visible on the lower side of the root compared with the upper side after 2 h and peaked at 3 h (Figures S4A and S4C). Quantitative analysis of fluorescence intensity ratios between the lower and upper sides confirmed significant differential expression (Figures S4B and S4D). Asymmetric expression of p*DR5*::Venus was evident in the lateral root cap and epidermis, whereas p*ARF19*::Venus expression appeared first in the epidermis, followed closely by the cortex, on the lower side of the root. Notably, no asymmetric expression p*ARF19*::Venus was observed in the lateral root cap (Figure 2B). Together, these results indicate that *ARF19* plays a role in integrating the auxin gradient into the asymmetric gene expression patterns required for gravitropic bending response.

Consistent with this, previous studies have shown that *ARF19* is the most responsive, activating (class A) ARF gene to auxin at the transcript level.[17] Supporting this, our transcript and reporter (p*ARF19*::GUS) analyses following IAA treatment revealed that *ARF19* expression is rapidly auxin-inducible (Figure S5). To

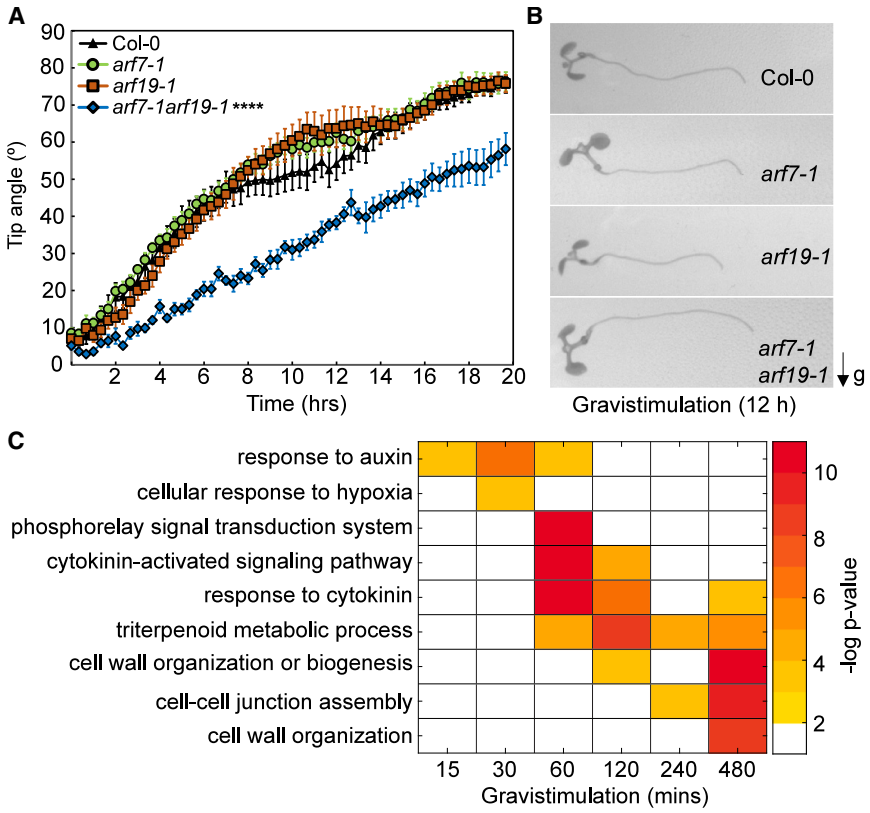

Figure 1. Auxin-related transcriptome changes precede a sequential induction of cytokinin and cell-wall-related processes during a root gravitropic response

(A and B) Root gravitropic response of 6-day-old *Arabidopsis thaliana* wild type (Col-0 ecotype) and *ARF7* and *ARF19* single and double mutants (*arf7-1*, *arf19-1* and *arf7-1 arf19-1*) after 90° gravistimulus. (A) Line graph showing root tip angle at every 15 min interval following 90° gravistimulas. Data represent mean ± standard errors from $n \geq 15$ seedlings. Statistical significance of differences in gravitropic bending responses over time between single mutants and the double mutant relative to Col-0 was assessed using Dunnett's T3 multiple comparisons test; no asterisk denotes no significant difference, whereas **** indicates a *p* value <0.0001. (B) Representative image showing bending response of Col-0, *arf7-1, arf19-1*, and *arf7-1 arf19-1* after 12 h of gravistimulus. *g* indicates gravity vector.

(C) Pruned version of GO enrichment analysis of differentially expressed genes from Col-0 and *arf7-1arf9-1* time series analyses, showing a cascade of events during root gravitropism.

determine the biological significance of this auxin-dependent amplification of *ARF19* during gravitropism, we expressed *ARF19* under the regulation of its native promoter in the *arf7-1arf19-1* background. As expected, the p*ARF19:ARF19* transgene was able to rescue the *arf7-1arf19-1* agravitropic phenotype (Figure 2D, bottom; Figure S6). However, when the three canonical auxin response elements (AuxREs) sequences encoded within the 3 kb promoter region were all mutated (Figure 2D, top), the modified p*ARF19:ARF19* transgene was no longer able to rescue the *arf7-1 arf19-1* gravitropic defect (Figure 2C, bottom; Figure S6). These findings demonstrate that auxin-inducible *ARF19* expression is essential for proper root gravitropism.

ARF19 auxin-inducible expression is partially dependent on ARF7

To dissect the regulatory relationship between ARF7 and ARF19, which are both required for gravitropism, where one is auxin-inducible (ARF19) and one is not (ARF7), we employed mathematical modeling to simulate how a downstream target output featuring different network topologies responds to a transient auxin input, in order to mimic a lateral auxin gradient following a gravitropic stimulus (see STAR Methods). As in any model of the auxin response, the core mechanism centers on auxin-triggered degradation of Aux/IAA proteins. In the absence of auxin, these proteins dimerize with ARF transcription factors, thereby repressing gene expression. When auxin levels increase, Aux/IAA proteins are degraded, thereby relieving repression and allowing ARFs to activate transcription. We tested three network topologies (Figure 3A). In topology 1, ARF7 is expressed at a basal level and is capable of binding its own promoter to auto-activate its expression (case1, Figure 3A). In topology 2, ARF7 cannot bind its own promoter but instead activates the production of ARF19, which in turn can auto-activate its expression (case2, Figure 3A). In topology 3, ARF7 activates ARF19, but neither ARF7 nor ARF19 can auto-activate. In topologies 2 and 3, ARF7 is assumed to be present at a constant basal level in both monomeric and dimeric forms. In all models, both ARF7

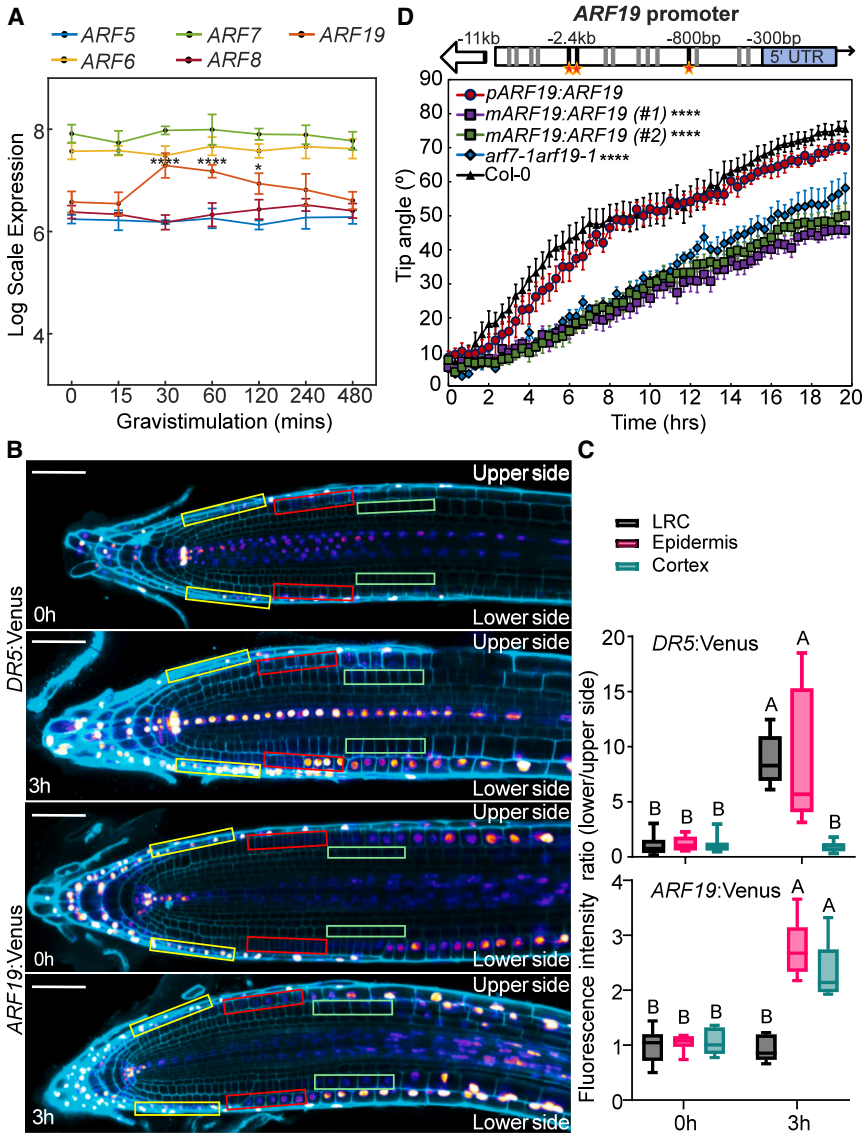

Figure 2. *ARF19* auxin-inducible expression is required for root gravitropism

(A) Expression of *ARF5, ARF6, ARF7, ARF8*, and *ARF19* mRNAs in the root tips at 0, 15, 30, 60, 120, 240, and 480 min following 90° gravistimulus. Data represent mean ± standard deviation from four biological replicates. Statistical significance was assessed by comparing each time point with the 0 min time point within each *ARF* expression series using a standard *t* test; * indicates *p* value <0.01 and **** indicates *p* value < 0.0001.

(B) Representative confocal images of 6 days old seedlings expressing the auxin response reporter *pDR5*::Venus (*DR5*:Venus) and the transcriptional reporter *pARF19*::3XVenus-NLS (*ARF19*:Venus) grown under 0 and 3 h of gravistimulus. Yellow, red, and cyan rectangles indicate subsequent regions of interests used to quantify fluorescence in the lateral root cap, epidermis, and cortex tissue types, respectively, on the lower and upper side of the roots of *DR5*:Venus and *ARF19*:Venus reporters. Scale bars, 50 μm.

(C) Boxplot showing the quantified ratios of fluorescence intensities between the lower and upper sides of bending roots of *DR5*::Venus and *ARF19*:Venus reporters after 0 and 3 h of gravistimulus in lateral root cap, epidermis and cortex tissue types. $n \geq 5$ seedlings per replicate, with two replicates. Statistical significance was assessed by two-way ANOVA; different letters indicate statistically significant differences between groups (*p* value <0.05).

(D) Top: showing schematic of *ARF19* promoter indicating core AuxREs (TGTC/GACA) in gray and canonical AuxREs (GAGACA/TGTCTC) in black. The stars indicate sites targeted for site-directed mutagenesis. Bottom: Line graph showing root tip angle at every 15 min interval following 90° gravistimulus of *arf7-1arf19-1* lines rescued with *ARF19* driven by its native promoter (*pARF19*) or by the mutated AuxREs form (*mARF19*). #1 and #2 indicate two independent lines.

Data represent mean ± standard errors from $n \geq 15$ seedlings. Statistical significance of differences in gravitropic bending responses over time between double mutant *arf7-1arf19-1* and *pARF19* and *mARF19* complementation lines relative to Col-0 was assessed using Dunnett's T3 multiple comparisons test; no asterisk denotes no significant difference, whereas **** indicates a *p* value <0.0001.

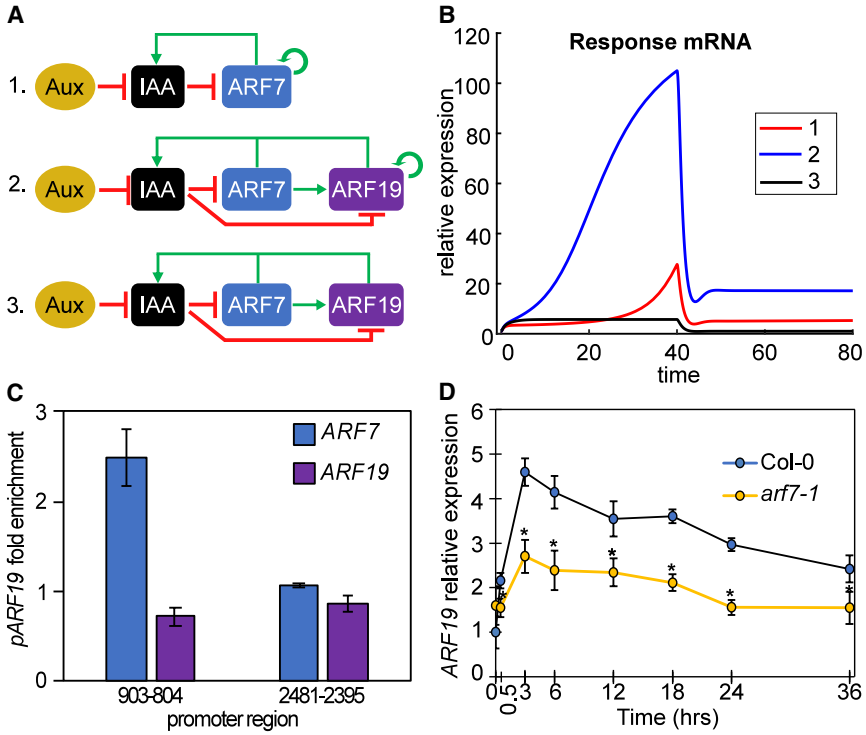

Figure 3. Auxin-inducible expression of *ARF19* during gravitropism is partially dependent on ARF7

(A) Three possible topologies (1–3) used to simulate the impact of network topology on auxin response. Red lines indicate post-translational repression, and green arrows indicate transcriptional upregulation. AUX, auxin; IAA, indole-3-acetic acid proteins, and ARF, auxin response factor.

(B) Example output (ARF7/19 target mRNA concentration, relative to the initial basal value) from modeling 3 topologies. Models are run from steady state at a basal level of auxin. Auxin is then increased at t = 0, then reduced back to the basal level at $t = 40$. In topology 1, the response is due to ARF7 only, while in topology 2 and 3, the response mRNA is activated by both ARF7 and ARF19, with and without self-activation of ARF19, respectively. These simulations identify that ARF7 regulates *ARF19* expression, and ARF19 does not auto-regulate.

(C) Anti-ARF7 and anti-ARF19 ChIP-qPCR showing that ARF7 binds the promoter of ARF19, but ARF19 does not bind its own promoter.

(D) Line graph showing RT-qPCR results of *ARF19* in Col-0 and *arf7-1* mutant following auxin treatment (1μM IAA) at 0, 0.5, 3, 6, 12, 18, 24, and 36 h time points. Data represent mean ± standard deviation from two biological replicates. Statistical significance was assessed by comparing each corresponding time point of *arf7-1* with Col-0 within the time series using a standard *t* test; * indicates *p* value <0.05.

and ARF19 (where present) can activate a generic Aux/IAA mRNA/protein (labeled IAA). A key assumption of the model is that both ARF7 and ARF19 (where present) can dimerize with themselves and with each other. These dimeric forms are assumed to be more powerful in activating transcription and have a greater affinity with the promoter than the monomeric versions and also have a greater affinity with the promoter than the Aux/IAA-ARF dimers.

All models were run from steady state at a basal level of auxin. Auxin was then increased at $t = 0$, then reduced back to basal level at $t = 40$. It is important to note that the simulation time axis represents simulated dynamic behavior rather than absolute biological time, and the model is intended to capture qualitative system dynamics rather than quantitatively identify experimental fold changes or time scales. For a network topology involving auto-activation of ARF7, we observed bi-stable behavior i.e., *ARF19* target mRNAs remain upregulated even after the auxin input is removed (Figure 3B, topology 1), as reported by Lau et al.[12] Similarly, for a network topology involving ARF19 activation by ARF7 with autoregulation of ARF19, we also observed bi-stability and much greater amplification of the auxin response output (Figure 3B, topology 2). For the network involving ARF19 activation by ARF7 where ARF19 cannot bind its own promoter, this topology did not exhibit bi-stable behavior, but instead featured a moderate activation of transcriptional response output rapidly switching off following the end of the temporary auxin stimulus (Figure 3B, topology 3). It is consistent with the transient activation of *ARF19* expression pattern observed in Figure 2A, where induction is followed by a return to basal levels. Hence, comparison of experimental and model simulations predicts that ARF7 controls ARF19 expression whilst ARF19 does not auto-regulate (as shown in network topology 3).

To directly validate the ARF7-ARF19 regulatory network topology (Figure 3A), we performed ARF7 and ARF19 ChIP-qPCR using primers to a region in close proximity to the AuxREs within the promoter of *ARF19* (Figure 2C, top). Our ChIP-qPCR results using ARF7 antibodies found enrichment using primers designed to amplify region −903 to 804; this was not the case with ARF19 antibodies (Figure 3C). This region is in close proximity to one of the mutated canonical AuxREs (−799), which is important for the expression of *ARF19* during the root gravitropism response (Figure 2C). No enrichment was found for ARF7 or ARF19

antibodies using primers designed to amplify region −2481 to 2395 (Figure 3C). Thus, ChIP-qPCR analysis revealed that ARF7, but not ARF19, binds the *ARF19* promoter at the tested regions to regulate its expression. While these data support the proposed regulatory relationship, we note that they do not formally exclude the possibility of ARF19 binding at other promoter regions. Thus, although our results are consistent with a lack of ARF19 autoregulation, this cannot be definitively ruled out without further experimental analysis. To test whether the auxin-inducible expression of ARF19 was solely dependent on ARF7, we performed RT-qPCR analysis of *ARF19* in *arf7-1* mutant vs. wild type following IAA treatment. The results revealed that, whilst *ARF19* mRNA abundance is significantly reduced in *arf7-1,* its temporal expression profile mimicked wild type, albeit at a lower level (Figure 3D). Hence, auxin-inducible expression of *ARF19* is only partially dependent on ARF7, and other ARFs may also bind the ARF19 promoter.

ARF7 and ARF19 co-regulate root gravitropism with ARF6 and ARF8

As *ARF19* expression is only partially dependent on ARF7, we asked whether additional activating (class A) ARFs contribute to the regulation of root gravitropism by acting redundantly with ARF7/19. In particular, ARF6 and ARF8 have been shown to function redundantly in other auxin-regulated processes, and their expression in the root tip overlaps with that of *ARF7* and *ARF19* (Figure S3) in tissues relevant to root gravitropism. We, therefore, probed their roles during root gravitropism by characterizing the gravitropic phenotypes of loss-of-function *arf6-1 and arf8-2* mutant alleles in combination with *arf7-1arf19-1*.

We observed that single *arf6-1* and *arf8-2* mutant alleles do not show defects (like single *arf7-1* and *arf19-1* mutant alleles; Figure 1B) in root gravitropism. However, the reduced gravity response of the *arf7-1arf19-1* double mutant is further enhanced by loss of either *ARF8* or *ARF6* (Figure 4A; Figure S7). Additionally, we observed a stronger phenotype for *arf7-1arf19-1arf8-2* compared with *arf7-1arf19-1arf6-1* mutant, which may suggest that ARF8 could have a more prominent role than ARF6 in root gravitropism. These analyses suggested that ARF7 and ARF19 could co-regulate root gravitropism together with ARF6 and ARF8.

To investigate this further, we tested whether ARF6 or ARF8 bind (like ARF7) the *ARF19* promoter. A public ARF6 ChIP-seq dataset[18] revealed that canonical AuxREs in the *ARF19* promoter at positions −2460, −2383, or −799 were not enriched, suggesting that ARF6 does not bind the *ARF19* promoter. Interestingly, ChIP-qPCR analysis identified that ARF8 cannot bind ARF19 promoter motifs at −2460 or −2383 but can bind motif at position −799 (Figure S8), which is important for ARF19-dependent gravitropism (Figure 2C). This suggests that ARF8 binds the *ARF19* promoter directly to regulate its auxin-inducible expression during root gravitropism, consistent with the stronger phenotype observed for *arf7-1arf19-1arf8-2*.

ARF19 and ARF7 are functionally distinct

ARF proteins have been shown to have both overlapping and non-redundant functions.[13,19,20] ARF19 is most closely related to ARF7[21] leading to suggestions that these ARFs are functionally redundant. However, our observation that ARF19 cannot bind the same *ARF19* promoter region as ARF7 (Figure 3C) suggests these ARFs have distinct binding specificities and, therefore, likely to be functionally distinct. To test this hypothesis, we generated *ARF7-GR* and *ARF19-GR* transgenes and examined the induction of target genes in roots of 5-day-old seedlings following 4 h treatments ± 2 uM dexamethasone (DEX) while growing on 1-naphthaleneacetic Acid (NAA) (see STAR Methods). As expected, ARF7 and ARF19 shared 22 DEX-induced downstream (direct as well as secondary) targets (Figure 4B). These targets included well-known auxin response genes, such as *Aux/IAAs* and *GH3s*, and previously published direct targets of both ARF7 and ARF19, such as *LBD16* and *LBD29*.[16] However, 277 and 27 upregulated target genes were specific to ARF7 and ARF19, respectively (Table S3), suggesting that they are functionally distinct.

To functionally assess their overlapping specificities, we expressed *ARF7* and *ARF19* under either their own or opposite promoters in the *arf7-1arf19-1* mutant background. Both *ARF7* and *ARF19* expressed under their own promoters were able to rescue the *arf7-1arf19-1* gravitropic defect (Figures 4C and 4D). Similarly, *ARF7* driven by the *ARF19* promoter was able to rescue the *arf7-1arf19-1* gravitropism defect. However, *ARF19* was not able to rescue *arf7-1arf19-1* when expressed using the *ARF7* promoter. Our functional analyses thus reveal that ARF7 can trans-complement ARF19 during gravitropism but not vice versa. Hence, ARF7 is likely to share overlapping target genes with ARF19 but also distinct functionally important targets such as *ARF19* itself. Furthermore, these analyses highlight the importance of auxin-inducible *ARF19* promoter activity to trigger specific temporal expression patterns of target genes to carry out a root gravitropic bending response.

DISCUSSION

Our transcriptome analysis indicates that root gravitropism involves a sequential, transient induction of genes involved in auxin, cytokinin, and cell-wall-related processes (Figure 1C). This cascade shows association with specific tissues and developmental stages of root growth. Firstly, expression patterns show that auxin-responsive genes are predominantly expressed in lateral root cap and epidermal cells in the meristematic and elongation regions, consistent with their roles in auxin transport and response.[2] Subsequently, genes associated with cytokinin signaling also appear to be expressed in epidermal cells in the elongation region, consistent with previous reports of cytokinins involvement in root gravitropic response.[22–24] For example, Pernisova et al.[25] proposed that cytokinins could influence AUX1-mediated auxin transport to control root gravitropism. However, our results suggest that cytokinin signaling and response genes could also be transcriptionally regulated downstream of the auxin response. Nevertheless, the exact crosstalk of these hormone pathways in elongating epidermal cells remains to be elucidated. Lastly, the upregulation of cell-wall-related genes appears largely confined to elongating cortical cells. This epidermis- and cortex-specific expression pattern seems consistent with the differential *ARF19* expression in these tissues

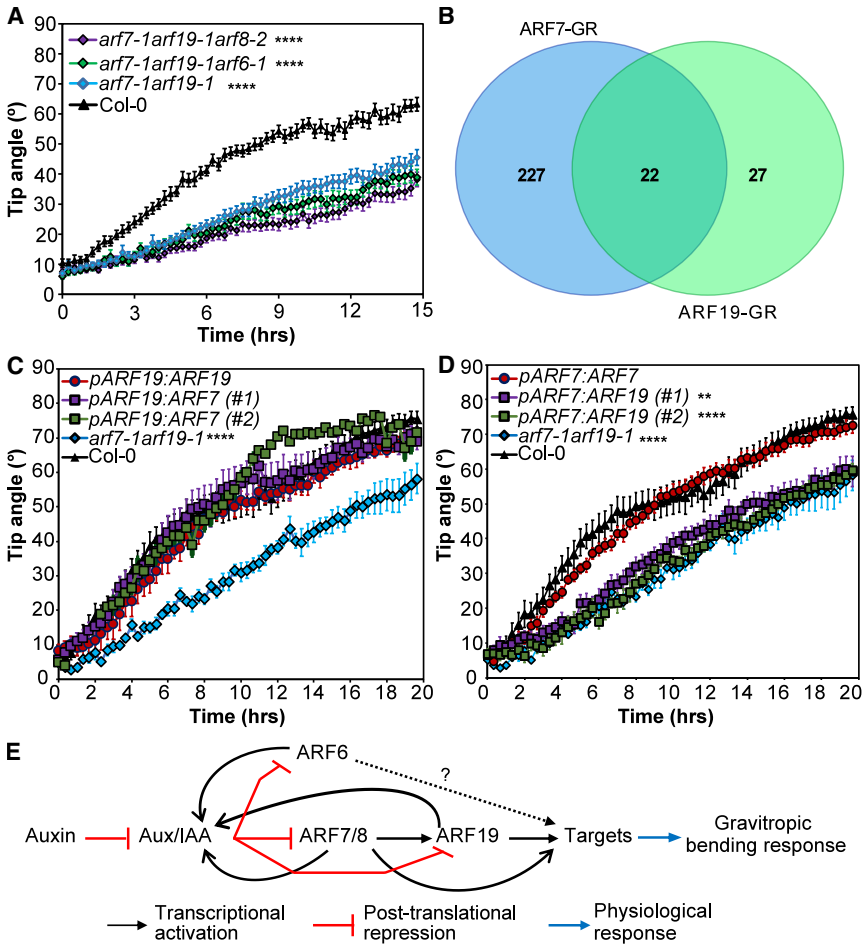

Figure 4. ARF7 and ARF8 co-regulate root gravitropism via upregulation of ARF19 expression

(A) Line graph showing root tip angle at every 15 min interval following 90° gravistimulus of Col-0, *arf7-1arf19-1*, *arf7-1arf19-1arf8-2*, and *arf7-1arf19-1arf6-1* lines.

(B) Venn analysis showing number of overlapping and non-overlapping target genes of ARF7 and ARF19.

(C and D) Line graph showing root tip angle at every 15 min interval following 90° gravistimulus of Col-0, *arf7-1arf19-1*, and *arf7-1arf19-1* lines rescued with (C) ARF19 driven by its native promoter (pARF19) and with ARF7 driven by ARF19 promoter and (D) ARF7 driven by its native promoter (pARF7) and but not by ARF19 driven by ARF7 promoter.

(E) Model of transcriptional network involved during root gravitropism. For (A), (C) and (D), #1 and #2 indicates two independent lines.

Data represent mean ± standard errors from $n \geq 15$ seedlings. Statistical significance of differences in gravitropic bending responses over time between individual lines relative to Col-0 was assessed using Dunnett's T3 multiple comparisons test; no asterisk denotes no significant difference, whereas ** indicates a p value <0.01 and **** indicates a p value <0.0001. For (A), we additionally tested statistical significance between *arf7-1arf19-1arf8-2* and *arf7-1arf19-1arf6-1* relative to *arf7-1arf19-1* and found that *arf7-1arf19-1arf8-2* is statistically significant (p value = 0.0225).

after a gravistimulus (Figure 2B). However, the precise temporal relationships among these pathways remain unresolved and require further investigation. Overall, our time series transcriptome dataset provides a strong foundation for further dissecting the role of spatiotemporally regulated genes during root gravitropism, but additional analyses will be necessary to confirm causal links.

The transient auxin response taking place at the start of a root gravitropic response is dependent on a sub-family of activating ARF transcription factors. Among the five activating ARFs in *Arabidopsis* sp., our time series transcriptome showed that only *ARF19* is rapidly and transiently induced following gravistimulation. This is consistent with previous reports that *ARF19* is the most responsive ARF to auxin treatment.[17] Our gravitropism transcriptome and auxin-treatment data indicate that auxin response is induced within 30 min, and that *arf7-1arf19-1* mutants consistently exhibit defects in the initiation of root curvature at early time points (Figure 1A; Figure S7A). Together, these results suggest that ARF19 plays a critical role in initiating the gravitropic bending response and contributes to the maintenance of curvature by regulating the expression of downstream targets. Previously ARF7 and ARF19 have both been shown to be required for root gravitropism.[13] As *ARF19* is auxin-inducible and *ARF7* is not, we asked how the transient regulation of *ARF19* is achieved during a gravitropic response. We discovered that a gene regulatory network featuring ARF19 activation by

ARF7, but where ARF19 is unable to auto-activate itself, is ideally suited to transiently induce a lateral auxin response gradient following a gravistimulus. Modeling revealed that this ARF network topology did not exhibit bi-stability, allowing auxin-regulated gene expression to rapidly switch on-off during root gravitropism, consistent with *ARF19* expression studies.

Our study revealed that ARF19 upregulation after a gravistimulus is partially dependent on ARF7 but also requires ARF6 and ARF8. These ARFs have previously been shown to co-regulate auxin-responsive target genes in non-root organs,[26] supporting the idea that functional redundancy among activating ARFs could be a common feature of auxin signaling. Our results suggest ARF19 is a direct target for (at least) ARF8 during a root gravitropic response. This regulatory model is consistent with ARF8 expression in root epidermal cells in meristematic and early elongation zones (Figure S3), where the ARF19 expression gradient is initiated during gravitropism. Thus, ARF7 and ARF8 may act in overlapping tissues to regulate or amplify ARF19 expression in response to auxin redistribution. In contrast, although ARF6 contributes to root gravitropism genetically, it does not appear to directly bind the ARF19 promoter, suggesting that ARF6 may regulate downstream auxin-responsive genes distinct from, or functionally related to, those controlled by ARF7 and ARF19. Together, these findings reveal that a more complex regulatory network of activating ARFs is required to control ARF19 and auxin response dynamics during root gravitropism than originally proposed.[13]

ARFs can form dimers (homo or hetero) or oligomers both through their DNA binding and specific protein-protein interaction domains,[27] suggesting the possibility of cooperative regulation. This notion is somewhat supported by results from our pARF19ARF19 complementation experiment in the *arf7-1arf19-1* background, which showed near complete, but not full, rescue of the gravitropic defect (Figure 2D). Further analysis revealed partial restoration of the lateral root phenotype and basal ARF19 expression levels; however, auxin-inducible expression was absent (Figure S9). These results imply that functional ARF7 is required for full auxin-mediated activation of ARF19 and that ARF8 alone is insufficient to compensate in its absence. Further, structural or biochemical studies would be required to dissect if ARF7 and ARF8 can cooperatively bind ARF19 promoter to regulate its auxin-dependent expression during a root gravitropic response.

Previous studies have reported that ARF proteins have both overlapping and non-redundant functions.[13,19,20] ARF7 and ARF19 are proposed to be functionally redundant as they are most closely related.[21] However, our study reveals that ARF7 and ARF19 have sub-functionalized, where ARF7 shares overlapping target genes with ARF19 but also has distinct functionally important targets such as ARF19 itself. This insight could also explain the distinct roles reported for ARF19 (compared with ARF7) including, for example, its role in promoting auxin-dependent root hair elongation in response to low external phosphate.[28] In the case of root gravitropism, *ARF19* upregulation appears to function as a tissue-specific rapid auxin response enhancer, delivering a rapid and transient induction for downstream transcriptional changes required during later stages of a gravitropic response. These downstream targets may include either specific targets of ARF19 or targets shared with ARF7, which remains to be untangled further. The differential rescue observed when ARF7 and ARF19 were expressed under each other's promoters further highlights the importance of precise spatial and temporal control of ARF activity in gravitropic response. ARF7 under the *ARF19* promoter successfully restored gravitropism in the *arf7-1 arf19-1* mutant, whereas ARF19 under the *ARF7* promoter did not. Although ARF7 and ARF19 share overlapping functions, their ability to substitute potentially depends on proper tissue localization and auxin-responsive expression. ARF19 driven by the *ARF7* promoter is likely expressed in wider tissues and zones, and no auxin inducibility may disrupt the tightly regulated asymmetric auxin response needed for asymmetric growth. In contrast, ARF7 under the auxin-inducible *ARF19* promoter is expressed in the correct tissues and responds quickly to auxin, enabling effective activation of downstream overlapping targets. Together, these results suggest that ARF19 primarily functions as an auxin-sensitive regulatory component, and ARF7 can substitute only within this correct regulatory context. Differences in expression levels or cofactor interactions may also contribute and need to be explored in future studies.

Overall, our results highlight a transcriptional network of activating ARFs featuring ARF7 and ARF8 activating auxin-inducible ARF19 expression (Figure 4E) to control a cascade of cellular processes in a highly spatiotemporally regulated manner during a root gravitropic response.

Limitations of the study

Although our higher-order mutant analyses and ChIP–qPCR results support a role for ARF8 in the proposed model, we did not examine auxin-inducible expression of *ARF19* in the *arf7-1 arf8-2* double mutant, nor did we assess the expression of well-established auxin-responsive genes, such as SAURs, Aux/IAAs, and GH3s, or downstream cytokinin or cell-wall-related genes induced during gravitropism in the *arf7-1arf19-1arf8-2* triple mutant. Analysis of these downstream responses would provide additional insight into how ARF7 and ARF8 contributes to auxin-regulated gene expression of target genes (including *ARF19*) and could help clarify regulatory relationships among ARF family members. Addressing these points in future studies will be important for further refining and strengthening the model presented here.

In addition, although the regulatory model is supported by our genetic, transcriptomic, and mathematical modeling analyses, direct experimental testing of alternative network configurations remains an important avenue for future work. Approaches that selectively modify ARF19 regulatory dynamics or upstream ARF7/8 activity would enable more rigorous evaluation of the proposed network architecture. Such studies could assess how changes in the timing, magnitude, or persistence of *ARF19* expression influence downstream transcriptional responses and gravitropic behavior. Systematic analyses of *ARF19* dynamics, downstream cytokinin and cell-wall-associated gene induction, and gravitropic kinetics under these conditions will be essential for distinguishing between alternative regulatory scenarios and strengthening causal links within the model. Together, these future efforts will help resolve the

transcriptional regulation underlying auxin-mediated root gravitropism.

RESOURCE AVAILABILITY

Lead contact

Requests for further information and resources should be directed to and will be fulfilled by the lead contact, Dr. Rahul Bhosale (rahul.bhosale@nottingham.ac.uk).

Materials availability

All materials generated in this study are available from the corresponding authors upon reasonable request.

Data and code availability

- All gravitropism timeseries transcriptomics data used in this paper are included as supplementary files. ARF7-GR and ARF19-GR datasets are deposited in ArrayExpress and are publicly available as of the date of publication. Accession numbers are listed in the key resources table.
- The details of mathematical model are included in the STAR Methods as this paper does not report original code.
- Any additional information required to reanalyze the data reported in this paper is available from the lead contact upon request.

ACKNOWLEDGMENTS

R.A.B. thanks Future Food Beacon Nottingham Research and BBSRC Discovery (BB/S011102/1) Fellowships and BBSRC New Investigator research (BB/X014843/1) and partner (BB/X018806/1) grants. E.M.S. and K.V. acknowledge the support of the National Research Foundation and the University of Antwerp. This work was supported by MEXT/JSPS KAKENHI grants 12J02079 to T. Goh and 19060006, 25113003, and 19H05673 to H.F., and by JST, PRESTO grant no. JPMJPR2144 to T. Goh J.T. acknowledges a joint INRA/University of Nottingham PhD grant and T.V. acknowledges ANR-2014-CE11-0018 grant (Serrations). J.O. acknowledges the support of R&D programme of "Plasma Advanced Technology for Agriculture and Food (code no.1711124797)" through the Korea Institute of Fusion Energy (KFE) funded by the Government funds, Republic of Korea. A.K. acknowledges support from the Republic of Türkiye Ministry of National Education and Ministry of Agriculture and Forestry and the Rank Prize Fund. B.K.P. acknowledges the support from the BBSRC Discovery Fellowship (No. BB/V00557X/1).

AUTHOR CONTRIBUTIONS

Conceptualization, R.A.B. and M.J.B.; methodology, E.G., T. Goh, K.H., N.M., E.M.S., and D.W.; formal analysis, M.W. and R.A.B.; resources, J.T., J.O., J.H., R.S., G.H., T. Guilfoyle, K.V., T.B., T.V., A. Bishopp, and H.F.; investigation, E.G., K.H., T. Goh, N.M., N.L., E.M.S., J.B., A.L., A.Bansod, B.K.P., A.K., and B.P.; writing – original draft, R.A.B. and M.B.; writing – review and editing, E.G., K.H., T. Goh, N.M., K.V., T.V., and A. Bishopp; funding acquisition, E.G., T. Goh, R.A.B., and M.J.B.; supervision, R.A.B. and M.J.B.

DECLARATION OF INTERESTS

The authors declare no competing interests.

STAR★METHODS

Detailed methods are provided in the online version of this paper and include the following:

SUPPLEMENTAL INFORMATION

Supplemental information can be found online at https://doi.org/10.1016/j.celrep.2026.117555.

Received: August 12, 2025
Revised: December 26, 2025
Accepted: May 27, 2026
Published: June 16, 2026

REFERENCES

1. Ottenschläger, I., Wolff, P., Wolverton, C., Bhalerao, R.P., Sandberg, G., Ishikawa, H., Evans, M., and Palme, K. (2003). Gravity-regulated differential auxin transport from columella to lateral root cap cells. Proc. Natl. Acad. Sci. USA *100*, 2987–2991. https://doi.org/10.1073/pnas.0437936100.
2. Swarup, R., Kramer, E.M., Perry, P., Knox, K., Leyser, H.M.O., Haseloff, J., Beemster, G.T.S., Bhalerao, R., and Bennett, M.J. (2005). Root gravitropism requires lateral root cap and epidermal cells for transport and response to a mobile auxin signal. Nat. Cell Biol. *7*, 1057–1065. https://doi.org/10.1038/ncb1316.
3. Band, L.R., Wells, D.M., Larrieu, A., Sun, J., Middleton, A.M., French, A.P., Brunoud, G., Sato, E.M., Wilson, M.H., Péret, B., et al. (2012). Root gravitropism is regulated by a transient lateral auxin gradient controlled by a tipping-point mechanism. Proc. Natl. Acad. Sci. USA *109*, 4668–4673. https://doi.org/10.1073/pnas.1201498109.
4. Boonsirichai, K., Guan, C., Chen, R., and Masson, P.H.; New Collective Author (2002). ROOT GRAVITROPISM: An Experimental Tool to Investigate Basic Cellular and Molecular Processes Underlying Mechanosensing and Signal Transmission in Plants. Annu. Rev. Plant Biol. *53*, 421–447. https://doi.org/10.1146/annurev.arplant.53.100301.135158.
5. Morita, M.T. (2010). Directional Gravity Sensing in Gravitropism. Annu. Rev. Plant Biol. *61*, 705–720. https://doi.org/10.1146/annurev.arplant.043008.092042.
6. Dharmasiri, N., Dharmasiri, S., and Estelle, M. (2005). The F-box protein TIR1 is an auxin receptor. Nature *435*, 441–445. https://doi.org/10.1038/nature03543.
7. Tan, X., Calderon-Villalobos, L.I.A., Sharon, M., Zheng, C., Robinson, C.V., Estelle, M., and Zheng, N. (2007). Mechanism of auxin perception by the TIR1 ubiquitin ligase. Nature *446*, 640–645. https://doi.org/10.1038/nature05731.
8. Kepinski, S., and Leyser, O. (2005). The Arabidopsis F-box protein TIR1 is an auxin receptor. Nature *435*, 446–451. https://doi.org/10.1038/nature03542.
9. Ramos, J.A., Zenser, N., Leyser, O., and Callis, J. (2001). Rapid Degradation of Auxin/Indoleacetic Acid Proteins Requires Conserved Amino Acids of Domain II and Is Proteasome Dependent. Plant Cell *13*, 2349–2360. https://doi.org/10.1105/tpc.010244.

10. Ulmasov, T., Murfett, J., Hagen, G., and Guilfoyle, T.J. (1997). Aux/IAA Proteins Repress Expression of Reporter Genes Containing Natural and Highly Active Synthetic Auxin Response Elements. Plant Cell *9*, 1963. https://doi.org/10.2307/3870557.

11. Vernoux, T., Brunoud, G., Farcot, E., Morin, V., Van den Daele, H., Legrand, J., Oliva, M., Das, P., Larrieu, A., Wells, D., et al. (2011). The auxin signalling network translates dynamic input into robust patterning at the shoot apex. Mol. Syst. Biol. *7*, 508. https://doi.org/10.1038/msb.2011.39.

12. Lau, S., De Smet, I., Kolb, M., Meinhardt, H., and Jürgens, G. (2011). Auxin triggers a genetic switch. Nat. Cell Biol. *13*, 611–615. https://doi.org/10.1038/ncb2212.

13. Okushima, Y., Overvoorde, P.J., Arima, K., Alonso, J.M., Chan, A., Chang, C., Ecker, J.R., Hughes, B., Lui, A., Nguyen, D., et al. (2005). Functional Genomic Analysis of the AUXIN RESPONSE FACTOR Gene Family Members in Arabidopsis thaliana: Unique and Overlapping Functions of ARF7 and ARF19. Plant Cell *17*, 444–463. https://doi.org/10.1105/tpc.104.028316.

14. Leyser, O. (2018). Auxin Signaling. Plant Physiol. *176*, 465–479. https://doi.org/10.1104/pp.17.00765.

15. Brady, S.M., Orlando, D.A., Lee, J.-Y., Wang, J.Y., Koch, J., Dinneny, J.R., Mace, D., Ohler, U., and Benfey, P.N. (2007). A High-Resolution Root Spatiotemporal Map Reveals Dominant Expression Patterns. Science *318*, 801–806. https://doi.org/10.1126/science.1146265.

16. Okushima, Y., Fukaki, H., Onoda, M., Theologis, A., and Tasaka, M. (2007). ARF7 and ARF19 Regulate Lateral Root Formation via Direct Activation of LBD/ASL Genes in Arabidopsis. Plant Cell *19*, 118–130. https://doi.org/10.1105/tpc.106.047761.

17. Paponov, I.A., Paponov, M., Teale, W., Menges, M., Chakrabortee, S., Murray, J.A.H., and Palme, K. (2008). Comprehensive Transcriptome Analysis of Auxin Responses in Arabidopsis. Mol. Plant *1*, 321–337. https://doi.org/10.1093/mp/ssm021.

18. Oh, E., Zhu, J.-Y., Bai, M.-Y., Arenhart, R.A., Sun, Y., and Wang, Z.-Y. (2014). Cell longation is regulated through a central circuit of interacting transcription factors in the Arabidopsis hypocotyl. eLife *3*, e03031. https://doi.org/10.7554/elife.03031.

19. Hardtke, C.S., Ckurshumova, W., Vidaurre, D.P., Singh, S.A., Stamatiou, G., Tiwari, S.B., Hagen, G., Guilfoyle, T.J., and Berleth, T. (2004). Overlapping and non-redundant functions of the Arabidopsis auxin response factors MONOPTEROS and NONPHOTOTROPIC HYPOCOTYL 4. Development *131*, 1089–1100. https://doi.org/10.1242/dev.00925.

20. Rademacher, E.H., Lokerse, A.S., Schlereth, A., Llavata-Peris, C.I., Bayer, M., Kientz, M., Freire Rios, A., Borst, J.W., Lukowitz, W., Jürgens, G., and Weijers, D. (2012). Different Auxin Response Machineries Control Distinct Cell Fates in the Early Plant Embryo. Dev. Cell *22*, 211–222. https://doi.org/10.1016/j.devcel.2011.10.026.

21. Remington, D.L., Vision, T.J., Guilfoyle, T.J., and Reed, J.W. (2004). Contrasting Modes of Diversification in the Aux/IAA and ARF Gene Families. Plant Physiol. *135*, 1738–1752. https://doi.org/10.1104/pp.104.039669.

22. Aloni, R., Langhans, M., Aloni, E., and Ullrich, C.I. (2004). Role of cytokinin in the regulation of root gravitropism. Planta *220*, 177–182. https://doi.org/10.1007/s00425-004-1381-8.

23. Philosoph-Hadas, S., Friedman, H., and Meir, S. (2005). Gravitropic Bending and Plant Hormones. Vitam. Horm. *72*, 31–78. https://doi.org/10.1016/s0083-6729(05)72002-1.

24. Singh, M., Gupta, A., and Laxmi, A. (2017). Striking the Right Chord: Signaling Enigma during Root Gravitropism. Front. Plant Sci. *8*, 1304. https://doi.org/10.3389/fpls.2017.01304.

25. Pernisova, M., Prat, T., Grones, P., Harustiakova, D., Matonohova, M., Spichal, L., Nodzynski, T., Friml, J., and Hejatko, J. (2016). Cytokinins influence root gravitropism via differential regulation of auxin transporter expression and localization in Arabidopsis. New Phytol. *212*, 497–509. https://doi.org/10.1111/nph.14049.

26. Nagpal, P., Ellis, C.M., Weber, H., Ploense, S.E., Barkawi, L.S., Guilfoyle, T.J., Hagen, G., Alonso, J.M., Cohen, J.D., Farmer, E.E., et al. (2005). Auxin response factors ARF6 and ARF8 promote jasmonic acid production and flower maturation. Development *132*, 4107–4118. https://doi.org/10.1242/dev.01955.

27. Chandler, J.W. (2016). Auxin response factors. Plant Cell Environ. *39*, 1014–1028. https://doi.org/10.1111/pce.12662.

28. Bhosale, R., Giri, J., Pandey, B.K., Giehl, R.F.H., Hartmann, A., Traini, R., Truskina, J., Leftley, N., Hanlon, M., Swarup, K., et al. (2018). A mechanistic framework for auxin dependent Arabidopsis root hair elongation to low external phosphate. Nat. Commun. *9*, 1409. https://doi.org/10.1038/s41467-018-03851-3.

29. Cho, H., Ryu, H., Rho, S., Hill, K., Smith, S., Audenaert, D., Park, J., Han, S., Beeckman, T., Bennett, M.J., et al. (2014). A secreted peptide acts on BIN2-mediated phosphorylation of ARFs to potentiate auxin response during lateral root development. Nat. Cell Biol. *16*, 66–76. https://doi.org/10.1038/ncb2893.

30. Oh, J., Wilson, M., Hill, K., Leftley, N., Hodgman, C., Bennett, M.J., and Swarup, R. (2020). Arabidopsis antibody resources for functional studies in plants. Sci. Rep. *10*, 21945. https://doi.org/10.1038/s41598-020-78689-1.

31. Lavenus, J., Goh, T., Guyomarc'h, S., Hill, K., Lucas, M., Voß, U., Kenobi, K., Wilson, M.H., Farcot, E., Hagen, G., et al. (2015). Inference of the Arabidopsis Lateral Root Gene Regulatory Network Suggests a Bifurcation Mechanism That Defines Primordia Flanking and Central Zones. Plant Cell *27*, 1368–1388. https://doi.org/10.1105/tpc.114.132993.

32. Clough, S.J., and Bent, A.F. (1998). Floral dip: a simplified method for-Agrobacterium-mediated transformation ofArabidopsis thaliana. Plant J. *16*, 735–743. https://doi.org/10.1046/j.1365-313x.1998.00343.x.

33. Brunoud, G., Wells, D.M., Oliva, M., Larrieu, A., Mirabet, V., Burrow, A.H., Beeckman, T., Kepinski, S., Traas, J., Bennett, M.J., and Vernoux, T. (2012). A novel sensor to map auxin response and distribution at high spatio-temporal resolution. Nature *482*, 103–106. https://doi.org/10.1038/nature10791.

34. Truskina, J., Han, J., Chrysanthou, E., Galvan-Ampudia, C.S., Lainé, S., Brunoud, G., Macé, J., Bellows, S., Legrand, J., Bågman, A.-M., et al. (2021). A network of transcriptional repressors modulates auxin responses. Nature *589*, 116–119. https://doi.org/10.1038/s41586-020-2940-2.

35. Schindelin, J., Arganda-Carreras, I., Frise, E., Kaynig, V., Longair, M., Pietzsch, T., Preibisch, S., Rueden, C., Saalfeld, S., Schmid, B., et al. (2012). Fiji: an open-source platform for biological-image analysis. Nat. Methods *9*, 676–682. https://doi.org/10.1038/nmeth.2019.

36. Maere, S., Heymans, K., and Kuiper, M. (2005). BiNGO: a Cytoscape plugin to assess overrepresentation of Gene Ontology categories in Biological Networks. Bioinformatics *21*, 3448–3449. https://doi.org/10.1093/bioinformatics/bti551.

37. Wells, D.M., French, A.P., Naeem, A., Ishaq, O., Traini, R., Hijazi, H.I., Bennett, M.J., and Pridmore, T.P. (2012). Recovering the dynamics of root growth and development using novel image acquisition and analysis methods. Philos. Trans. R. Soc. Lond. B Biol. Sci. *367*, 1517–1524. https://doi.org/10.1098/rstb.2011.0291.

38. Irizarry, R.A., Hobbs, B., Collin, F., Beazer-Barclay, Y.D., Antonellis, K.J., Scherf, U., and Speed, T.P. (2003). Exploration, normalization, and summaries of high density oligonucleotide array probe level data. Biostatistics *4*, 249–264. https://doi.org/10.1093/biostatistics/4.2.249.

39. Gentleman, R.C., Carey, V.J., Bates, D.M., Bolstad, B., Dettling, M., Dudoit, S., Ellis, B., Gautier, L., Ge, Y., Gentry, J., et al. (2004). Bioconductor: open software development for computational biology and bioinformatics. Genome Biol. *5*, R80. https://doi.org/10.1186/gb-2004-5-10-r80.

40. Smyth, G.K. (2004). Linear Models and Empirical Bayes Methods for Assessing Differential Expression in Microarray Experiments. Stat. Appl. Genet. Mol. Biol. *3*, Article3-25. https://doi.org/10.2202/1544-6115.1027.

41. Hochberg, Y., and Benjamini, Y. (1990). More powerful procedures for multiple significance testing. Stat. Med. *9*, 811–818. https://doi.org/10.1002/sim.4780090710.

42. Benjamini, Y., and Hochberg, Y. (1995). Controlling the False Discovery Rate: A Practical and Powerful Approach to Multiple Testing. J. Roy. Stat. Soc. B *57*, 289–300. https://doi.org/10.1111/j.2517-6161.1995.tb02031.x.

43. Nakagawa, T., Kurose, T., Hino, T., Tanaka, K., Kawamukai, M., Niwa, Y., Toyooka, K., Matsuoka, K., Jinbo, T., and Kimura, T. (2007). Development of series of gateway binary vectors, pGWBs, for realizing efficient construction of fusion genes for plant transformation. J. Biosci. Bioeng. *104*, 34–41. https://doi.org/10.1263/jbb.104.34.

44. Middleton, A.M., King, J.R., Bennett, M.J., and Owen, M.R. (2010). Mathematical Modelling of the Aux/IAA Negative Feedback Loop. Bull. Math. Biol. *72*, 1383–1407. https://doi.org/10.1007/s11538-009-9497-4.

45. Mellor, N., Bennett, M.J., and King, J.R. (2016). GH3-Mediated Auxin Conjugation Can Result in Either Transient or Oscillatory Transcriptional Auxin Responses. Bull. Math. Biol. *78*, 210–234. https://doi.org/10.1007/s11538-015-0137-x.

STAR★METHODS

KEY RESOURCES TABLE

REAGENT or RESOURCE	SOURCE	IDENTIFIER
Antibodies		
ARF19	Cho et al.[29]; Oh et al.[30]	N/A
ARF7	Lavenus et al.[31]	N/A
ARF8	This paper	N/A
Bacterial and virus strains		
Agrobacterium tumefaciens GV3101 (pMP90)	Clough et al.[32]	N/A
Biological samples		
p*DR5*::Venus	Vernoux et al.[11]	https://arabidopsis.info/StockInfo?NASC_id=73937
p*ARF5*:3xmVenus-NLS	Brunoud et al.[33]; Truskina et al.[34]	N/A
p*ARF6*:3xmVenus-NLS	Brunoud et al.[33]; Truskina et al.[34]	N/A
p*ARF7*::3×mVenus-NLS	Brunoud et al.[33]; Truskina et al.[34]	N/A
p*ARF8*:3xmVenus-NLS	Brunoud et al.[33]; Truskina et al.[34]	N/A
p*ARF19*::3×mVenus-NLS	Brunoud et al.[33]; Truskina et al.[34]	N/A
arf6-1arf7-1arf19-1	This paper	N/A
arf7-1arf8-2arf19-1	This paper	N/A
arf7-1	Okushima et al.[13]	https://arabidopsis.info/StockInfo?NASC_id=24607
arf19-1	Okushima et al.[13]	https://arabidopsis.info/StockInfo?NASC_id=24617
arf6-1	Okushima et al.[13]	https://arabidopsis.info/StockInfo?NASC_id=24606
arf8-2	Okushima et al.[13]	https://arabidopsis.info/StockInfo?NASC_id=24608
pARF7:ARF7:4xMyc	This paper	N/A
pARF7:ARF19:4xMyc	This paper	N/A
pARF19:ARF19:T7	This paper	N/A
pARF19:ARF7:T7	This paper	N/A
Col-0	NASC	N/A
Chemicals, peptides, and recombinant proteins		
Murashige and Skoog (MS)	Sigma-Aldrich	**NACRES:** NA.72 **UNSPSC Code:** 12352207
Invitrogen™ Dynabeads™ Protein G for Immunoprecipitation	Fisher Scientific (Invitrogen™)	**Product Code:** 10446293
Critical commercial assays		
Plant RNeasy Micro Kit	Qiagen	Cat no./ID. 74904
Affymetrix IVT-Express	Affymetrix	N/A
Transcriptor first-strand cDNA synthesis kit (Roche)	Sigma-Aldrich (Roche)	**UNSPSC Code:** 41106313 **NACRES:** NA.54
Roche Diagnostics LightCycler 480 SYBR Green I Master	Fisher Scientific (Roche)	**Product** Code.15317906

(*Continued on next page*)

Continued

REAGENT or RESOURCE	SOURCE	IDENTIFIER
Deposited data		
ARF7-GR (transcriptomics)	Lavenus et al.[31]	accession no. E-MTAB-3451 on ArrayExpress
ARF19-GR (transcriptomics)	This paper	accession no. E-MTAB-3451 on ArrayExpress
Oligonucleotides		
pro*ARF19* -903- to −804 Fw: GGTGCTCCATTGCGTATCA	This paper	N/A
pro*ARF19* -903- to −804 Rv: ACATGTCCGTATAATGCGAGAA	This paper	N/A
pro*ARF19* -2481 to-2395 Fw: GTGTGGTTACGATGAGGAGAAG	This paper	N/A
pro*ARF19* -2481 to-2395 Rv: CGACCGAGTCTTTCGGTTTAG	This paper	N/A
TUB3 control Fw: TGCATTGGTACACAGGTGAGGGAA	This paper	N/A
TUB3 control Rv: AGCCGTTGCATCTTGGTATTGCTG	This paper	N/A
arf6-1 Fw + LB: ATAATGAATGGAAGTTCAGGC	SALK	N/A
arf6-1 Rev: CATCAAAGGCAAAGGCAAAT	SALK	N/A
arf7-1 Fw: TCCTGCTGAGTTTGTGGTTCCTT	SALK	N/A
arf7-1 Rev: TGTTGCACTCCTCTTTGAACC	SALK	N/A
arf8-2 Fw: GATTGTACGGAAAAATTAGGG	SALK	N/A
arf8-2 Rev: CATCAAATCAGAATTATGGGA	SALK	N/A
arf19-1 Fw: TTTTTCAGGTTGCAGCATCG	SALK	N/A
arf19-1 Rev: GAGGTTTGGGGATTGGAAGTTCA	SALK	N/A
ARF19 qPCR Fw: GACATATCTATCGAGGCCAACC	This paper	N/A
ARF19 qPCR Rv: ACTGAATCACCCGCAAATAGT	This paper	N/A
UBA Control qPCR Fw: AGTGGAGAGGCTGCAGAA	This paper	N/A
UBA Control qPCR Rv: CTCGGGTAGCACGAGCTT	This paper	N/A
Software and algorithms		
Fiji	Schindelin et al.[35]	https://imagej.net/software/fiji/downloads
BINGO	Maere et al.[36]	https://apps.cytoscape.org/apps/bingo
Limma	Bioconductor	https://www.bioconductor.org/packages//release/bioc/vignettes/limma/inst/doc/intro.html
MATLAB	MathWorks	https://www.mathworks.com/products/matlab.html

EXPERIMENTAL MODEL AND STUDY PARTICIPANT DETAILS

Plant material

Arabidopsis thaliana ecotype Columbia 0 (Col-0) was used as the wildtype in all experiments. *arf7-1arf19-1* double mutant, previously described in,[13] was used for generating complementation lines (see below) and for all gravitropism experiments. *arf6-1*, *arf7-1*, *arf8-2* and *arf19-1* single mutants were used for gravitropism experiments and for creating triple knockout mutants (*arf7-1arf19-1arf8-2* and *arf7-1arf19-1arf6-1*). Col-0, *arf7-1*, *arf8-2*, previously described in,[13] were used for auxin treatment experiments. DR5:Venus, p*ARF5*:3xmVenus-NLS, p*ARF6*:3xmVenus-NLS, p*ARF7*:3xmVenus-NLS, p*ARF8*:3xmVenus-NLS, p*ARF19*:3xmVenus-NLS, previously described in,[33,34] were used for confocal experiments. All mutant lines were confirmed using primers listed in (Table S4).

Growth conditions

Seeds were surface sterilised with 70% ethanol for 5 mins and 100% ethanol for 30 s followed by five washes with sterile water and stratified at 4°C for 48 hours in dark. For all gravitropism experiments, seeds were germinated onto half-strength Murashige and Skoog (MS) medium supplemented with 1% Agar at pH 5.7 in growth room (22°C, continuous light; 125–150 μmol m^{-2} s^{-1}) and grown vertically for 6–7 days. Plates were then subjected to 90° stimulation and images were taken in 12/12 h dark/light conditions using robotic imaging facility at the University of Nottingham[37] for 24 h at interval of 15 min.

METHOD DETAILS

Root dissection, total RNA-extraction, and preparation

To facilitate the root dissection, sterile 100μm 9 × 9 cm nylon mesh pieces were disposed onto the media before sowing. Plates were stored in the dark in a vertical position at 4°C for 3 days and were subsequently transferred to a growth chamber at 22°C with a 24-h light regime of 150 μmol m^{-1} s^{-1}. Plates with seven-day old seedlings were subjected to 90° stimulation. The root tip to the first root hair bulge of the wild-type and *arf7-1 arf19-1* double mutant were harvested over a time-course comprising seven time points: 0, 15, 30, 60, 120, 240 and 480 min after gravistimulation. Each time series had four biological replicates. For each time point of a biological replicate, 200 root tips were harvested and immediately frozen in liquid nitrogen. Total RNA was extracted with the Plant RNeasy Micro Kit (Qiagen, Crawley, UK), including on-column DNA digestion to eliminate genomic DNA from the samples.

Array hybridization, labeling and data acquisition

The RNA samples were labeled with the Affymetrix IVT-Express labeling kit following standard Affymetrix protocols (Affymetrix, Santa Clara, CA, USA). RNA labeling and hybridization to Affymetrix ATH1 arrays were conducted by the Nottingham Arabidopsis Stock Center (NASC)'s International Affymetrix Service. Fifty-six independent hybridization experiments with four biological replicates were performed in this work. After the hybridization was performed, the emitted fluorescent signals were digitalized and read with the GeneChip Scanner 3000 7G (Affymetrix). Data acquisition was done with the GeneChip Command Console.

Microarray data analysis

The raw microarray data (.CEL) of Col-0 and *arf7-1arf19-1* timeseries were pre-processed together using the robust multichip average (RMA) normalization approach (background correction, quantile normalization, and summarization) implemented in the Bioconductor R package, version 2.5.[38,39] The Bioconductor package Limma was used to identify differentially expressed genes ($-1.5 \leq$ Fold Change ≥ 1.5). Pairwise comparisons between each timepoint with 0min timepoint for Col-0 timeseries and respective timepoint of *arf7-1arf19-1* vs. Col-0 timeseries were performed using moderated *t*-statistics and the eBayes method as implemented in Limma.[40] *p* values were corrected for multiple testing using the Benjamini-Hochberg method[41] at an FDR threshold of 0.05.

GO enrichment analyses

Functional enrichment results reported in this study were calculated with the BiNGO tool[36] using hypergeometric tests and Benjamini-Hochberg[42] multiple testing correction at FDR = 0.05. GO information and annotations for Arabidopsis were obtained from the GO database (www.geneontology.org; version downloaded on 11/11/2020). The 21,517 genes in the pre-processed Affymetrix ATH1 microarray dataset were used as the reference set for the GO enrichment analyses presented in figures (Figure 1C; Figure S1) and Table S2. The 21,517 genes listed in Table S5 were used as the reference set for all other analyses.

Plasmid construction and plant transformation

For pARF7:ARF7:4xMyc, pARF7:ARF19:4xMyc, pARF19:ARF19:T7 and pARF19:ARF7:T7, *ARF7* and *ARF19* promoters (about 2.4 kb) were inserted in front of gateway cassette of pGWB16 or pGWB25, respectively.[43] ARF7 and ARF19 coding regions were subsequently transferred from the pDONR221 vectors by Gateway LR recombination. Mutagenesis of AuxRE in ARF19 promoter was

performed by PCR-based site-directed mutagenesis method. The resulting vectors were introduced into *Agrobacterium tumefaciens* GV3101 (pMP90), and *arf7-1arf19-1* plants were transformed by floral dipping.[32]

Confocal imaging of ARF reporters

Seeds of reporter lines of auxin response (p*DR5*:Venus) and auxin response factors (p*ARF5*:3xmVenus-NLS, p*ARF6*:3xmVenus-NLS, p*ARF7*:3xmVenus-NLS, p*ARF8*:3xmVenus-NLS and p*ARF19*:3xmVenus-NLS) were sterilised and stratified as described above in growth conditions and grown vertically for 6 days on 1% Agar plates supplemented with ½ MS media. For gravistimulation, plates were turned 90° in dark conditions and 3–5 individual seedlings from each reporter lines were imaged at 0 and 3 h timepoints using SP5 confocal imaging suite (Leica).

ChIP-qPCR assays

A ChIP assay was performed on Col-0 using 2–3 g root tissue pretreated with 1 μM NAA and fixed under vacuum with 1% formaldehyde for 15 min. Nuclei were extracted and ChIP was performed, using anti-ARF19 antibody,[29,30] anti-ARF7 antibody[31] or anti-ARF8 antibody (in this study) following the method as described previously.[29,30] The anti-ARF8 antibody was generated in rabbits using an *Escherichia coli*-expressed antigenic region from amino acids 649 to 811 that was also used to affinity purify the resulting antiserum. The antibody detected a band of the correct size in Col-0 nuclei preps that was absent in *arf8* (Figure S10). Briefly, 200 μL of sheared chromatin (average fragment size of 400 bp) was added to 1 mL Immunoprecipitation Buffer (50 mM HEPES, pH 7.5, 150 mM KCl, 5 mM MgCl2, 0.1% Triton X-100) and incubated along with 3 μg of anti-ARF19 or anti-ARF7 at 4°C. Protein G Dynabeads (Invitrogen) were then added and further incubated at 4°C overnight. Input and ARF19 or ARF7 immunoprecipitated DNA was used for qPCR with SYBR green master mix and oligonucleotide primers. Oligos were designed for two regions of the ARF19 promoter containing Auxin Responsive Elements (AuxREs) likely corresponding to ARF binding sites (see Figure 2C; top). Antibody immunoprecipitated DNA is normalized to input chromatin using an internal control (TUB3) not bound by ARF antibodies. All qPCR reactions were performed as triplicate technical replicates using a Light Cycler 480 qPCR machine and are representative of three biological repeats. Genomic-PCR and RT-PCR were performed as previous described,[29,31] using primers listed in Table S4.

Auxin treatment and qRT-PCR analysis

For *ARF19* expression analysis in Col-0 and *arf7-1* mutant (Figure 3D), 10-day old seedlings were pre-treated with 1μM IAA for the 0, 3, 6, 12, 18, 24 and 36 h timepoints. Total RNA was extracted from roots using the RNeasy kit (Qiagen) with on-column DNAse treatment (RNAse free DNAse set, Qiagen). Poly(dT) cDNA was prepared from 1 μg total RNA using the Transcriptor first-strand cDNA synthesis kit (Roche). Quantitative PCR was performed using SYBR Green I mix (Roche) on a Roche LightCycler 480 apparatus. For *ARF19* expression analysis in Col-0, *arf7-1arf19-1* and *ARF19* complementation (in *arf7-1arf19-1* mutant background) with native and mutated AuxRE promoters (Figure S5), seedlings were treated with 1μM IAA for 2 h. RNA extraction and qRT-PCR were carried out as described above.

ARF7-GR and ARF19-GR microarray analysis

The ARF7-GR and ARF19-GR transcriptomic datasets were obtained using *pARF7:ARF7:GR* and *pARF19:ARF19:GR*, both in *nph4-1arf19-1* mutant backgrounds.[16] Experimental setup and DNA microarray generation and data analysis of downstream targets of ARF7 and ARF19 was performed as detailed in methods and supplemental methods-3 sections of Lavenus et al.[31] ARF7-GR dataset was published in Lavenus et al.[31] and both datasets can be accessed through the accession no. E-MTAB-3451 on ArrayExpress (www.ebi.ac.uk/arrayexpress). ARF7 and ARF19 direct and indirect targets are included in Table S3.

Mathematical modeling

The mathematical model is encoded, run and plotted using MATLAB, with the ode15s solver. To establish the initial 'basal' state of the simulation, the model was run from zero initial conditions for large t (with the exception of ARF7 protein, $[A7] = 0.25$), with the level of auxin = 0.001. At $t = 0$ in the plot shown (Figure 3B), auxin is increased to auxin = 1 until $t = 40$, when the level of auxin is reset to auxin = 0.001.

Model Formulation

The models and assumptions are based on previously published approaches to modeling the auxin response.[12,44,45] We consider 3 model variations.

1. ARF7 activates the response gene alone. ARF7 auto-activated.
2. ARF7 and ARF19 activate the response gene, ARF19 activated by both ARF7 and ARF19. ARF7 constitutive.
3. ARF7 and ARF19 activate the response gene, ARF19 activated by ARF7 only. ARF7 constitutive.

Model variables

All quantities are dimensionless, concentrations, time and so should be considered relative values. $[A7_m]$ (ARF7 mRNA) is not present in models (2) and (3), ARF19 mRNA and protein, and various complexes are not present in model (1).

Variable	Description	Model
[A7]	ARF7 protein	1,2,3
[A7:IAA]	ARF7 and Aux/IAA dimer	–
[IAA]	Generic Aux/IAA protein	–
[IAA_m]	Aux/IAA mRNA	–
[A7:A7]	ARF7 homodimers	–
[$A7_m$]	ARF7 mRNA	1
[A19]	ARF19 protein	2,3
[$A19_m$]	ARF19 mRNA	–
[A19:IAA]	ARF19 and Aux/IAA dimer	–
[A19:A19]	ARF19 homodimers	–
[A7:A19]	ARF7 ARF19 heterodimers	–

Model parameters

To minimise the number of model parameters, where possible each parameters represents a *type* of process, rather than individual values for each separate interaction. For example, there is a single parameter, μ_r, representing mRNA turnover rather than a separate value for each individual mRNA. Similarly, the binding threshold parameters (θ_a for activators, θ_d for dimer activators, and θ_r for dimer repressors) are shared for all promoters represented in the models. A full list of model parameters, with descriptions is given in the table below.

Parameter	Default value	Description
q	2	balance between bound/unbound ARF and Aux/IAA
z	2	balance between bound/unbound ARF dimers
K_{aux}	0.05	auxin concentration giving half maximum Aux/IAA degradation
auxin	0.001	current auxin concentration
d_t	1000	rate constant for dimerisation processes
μ_r	1	turnover rate of mRNAs
η_i	20	production rate of Aux/IAA protein
η_a	1	production rate of ARF protein
θ_a	20	promoter binding threshold for ARF monomers
θ_d	2	promoter binding threshold for ARF dimers
θ_r	20	promoter binding threshold for ARF and Aux/IAA dimers
λ	5	relative rate of translation due to dimer binding compared to monomers
a_0	0.0425	basal ARF7 transcription rate

Model equations

Model 1: ARF7 auto-activation

$$\frac{d[A7]}{dt} = \eta_a([A7_m] - [A7]) + d_t\left([A7:IAA] - q[A7][IAA] + 2\left([A7:A7] - z[A7]^2\right)\right)$$

$$\frac{d[A7:IAA]}{dt} = d_t(q[A7][IAA] - [A7:IAA])$$

$$\frac{d[IAA]}{dt} = \eta_i\left([IAA_m] - [IAA]\frac{auxin}{auxin+K_{aux}}\right) + d_t([A7:IAA] - q[A7][IAA])$$

$$\frac{d[IAA_m]}{dt} = \mu_r(F - [IAA_m])$$

$$\frac{d[A7:A7]}{dt} = d_t\left(z[A7]^2 - [A7:A7]\right)$$

$$\frac{d[R_m]}{dt} = \mu_r(F - [R_m])$$

$$\frac{d[A7_m]}{dt} = \mu_r(a_0 + F - [A7_m])$$

where:

$$F \equiv \frac{\frac{[A7]}{\theta_a} + \lambda\frac{[A7:A7]}{\theta_d}}{1 + \frac{[A7]}{\theta_a} + \frac{[A7:A7]}{\theta_d} + \frac{[A7:IAA]}{\theta_r}}$$

Model 2: ARF7 activates ARF19, ARF19 auto-activates

$$\frac{d[A7]}{dt} = d_t\left([A7:IAA] - q[A7][IAA] + 2\left([A7:A7] - z[A7]^2\right) + [A7:A19] - z[A7][A19]\right)$$

$$\frac{d[A7:IAA]}{dt} = d_t(q[A7][IAA] - [A7:IAA])$$

$$\frac{d[IAA]}{dt} = \eta_i\left([IAA_m] - [IAA]\frac{auxin}{auxin + K_{aux}}\right) + d_t([A7:IAA] - q[A7][IAA] + [A19:IAA] - q[A19][IAA])$$

$$\frac{d[IAA_m]}{dt} = \mu_r(G - [IAA_m])$$

$$\frac{d[A7:A7]}{dt} = d_t\left(z[A7]^2 - [A7:A7]\right)$$

$$\frac{d[A19_m]}{dt} = \mu_r(G - [A19_m])$$

$$\frac{d[A19]}{dt} = \eta_a([A19_m] - [A19]) + d_t\left([A19:IAA] - q[A19][IAA] + 2\left([A19:A19] - z[A19]^2\right) + [A7:A19] - z[A7][A19]\right)$$

$$\frac{d[A19:IAA]}{dt} = d_t(q[A19][IAA] - [A19:IAA])$$

$$\frac{d[A19:A19]}{dt} = d_t\left(z[A19]^2 - [A19:A19]\right)$$

$$\frac{d[A7:A19]}{dt} = d_t(z[A7][A19] - [A7:A19])$$

$$\frac{d[R_m]}{dt} = \mu_r(G - [R_m])$$

where:

$$G \equiv \frac{\frac{[A7]+[A19]}{\theta_a} + \lambda\frac{[A7:A7]+[A7:A19]+[A19:A19]}{\theta_d}}{1 + \frac{[A7]+[A19]}{\theta_a} + \frac{[A7:A7]+[A7:A19]+[A19:A19]}{\theta_d} + \frac{[A7:IAA]+[A19:IAA]}{\theta_r}}$$

Model 3: ARF7 activates ARF19, ARF19 not auto-activated.

As model 2, except the equation for $[A19_m]$ is replaced by:

$$\frac{d[A19_m]}{dt} = \mu_r(F - [A19_m])$$

Where, as before:

$$F \equiv \frac{\frac{[A7]}{\theta_a} + \lambda\frac{[A7:A7]}{\theta_d}}{1 + \frac{[A7]}{\theta_a} + \frac{[A7:A7]}{\theta_d} + \frac{[A7:IAA]}{\theta_r}}$$

QUANTIFICATION AND STATISTICAL ANALYSIS

Total RNA quantification

RNA was quantified by using a NanoDrop ND100 spectrophotometer (Nanodrop, Wilimington, USA) at 260nm wavelength and assessed for quality and concentration with a BioAnalyzer 2100 (Agilent, CA, USA). RNA was diluted with RNase-free water to make a final concentration of 50 ng μL^{-1}.

Confocal images quantification

Images were post-processed using Fijisoftware.[35] >2 biological replicates were performed for all reporter lines.

For tissue-specific quantification of p*DR5*:Venus, p*ARF7*:3×mVenus-NLS, and p*ARF19*:3×mVenus-NLS, more than eight seedlings were imaged along the longitudinal axis at the center of the root at 0 h and 3 h following gravistimulation using a Leica SP5 confocal microscope. Regions of interest (ROIs) included approximately five lateral root cap cells adjacent to the quiescent center (QC), followed by five epidermis cells and subsequently five cortical cells. Fluorescence intensity was quantified separately on the lower and upper sides of the root and normalised to the area of each ROI. A lower-to-upper fluorescence intensity ratio was then calculated and used to generate the graphs shown in Figure 2.

For analysis of the temporal dynamics of pDR5Venus and pARF193×mVenus-NLS, additional imaging was performed at 0, 1, 2, and 3 h following gravistimulation, and the same methodology was used to quantify tissue-specific expression asymmetry between the lower and upper sides of the root and used to generate the graphs shown in Figure S4.

For z stack image analysis of p*DR5*:Venus, p*ARF7*::3xmVenus-NLS and p*ARF19*::3xmVenus-NLS, more than 8 seedlings were imaged at 0 and 3 h timepoints after gravistimulation using SP5 confocal imaging suite (Leica). Each z stack consisted of 20 optical slices, which were individually post-processed using Fiji to quantify the fluorescence intensity to quantify the upper and lower sides of the root and normalised to the area of the region of interest (ROI), defined as the visible region on the respective side within each slice. A lower-to-upper fluorescence ratio was then calculated for each slice. Ratios from 20 slices were averaged to obtain a mean value per seedling, which were used to generate the Figure S5.

For z stack maximum projection image analysis of p*ARF7*:3×mVenus-NLS and p*ARF19*:3×mVenus-NLS, more than eight seedlings per reporter line were imaged at 0 h and 2 h after treatment with 1 μM IAA using a Leica SP5 confocal microscope. Each z stack consisted of 20 optical sections, which were used to generate maximum-intensity projection images. Fluorescence intensity was quantified per seedling from the maximum projections using Fiji across the entire root and normalised to the area of the region of interest (ROI). These values were used to generate the graphs shown in Figure S6.

qRT-PCR quantification

Target quantifications were performed with specific primer pairs Expression levels were normalised to an internal control (ubiquitin-associated gene UBA) (see Table S4). All qRT–PCR experiments were performed in triplicates, and the values represent Means ± SEM (standard error of means).

Statistical analysis

t test statistical analyses were performed in Excel. ANOVA and Dunnett's T3 multiple comparisons test statistical analyses were performed in GraphPad Prism. The precise statistical tests can be found in the corresponding Figure legend.